Int. J. Electrochem. Sci., 15 **(2020)** 8459 – 8470, doi: 10.20964/2020.09.45

International Journal of
ELECTROCHEMICAL
SCIENCE
www.electrochemsci.org

Mesoporous Nitrogen Doped Zinc Oxide Nanosheets with Enhanced Photocatalytic Activity

Renqing Guo[1], *Yan Lin*[1,2], *Yiqi Cao*[1], *Xiaohua Huang*[1,*]

[1] Department of Materials Engineering, Taizhou University, Taizhou 318000, China
[2] State Key Laboratory of Silicon Materials, Zhejiang University, Hangzhou 310027, China
[*]E-mail: huangxh@tzc.edu.cn

Received: 13 May 2020 / *Accepted:* 1 July 2020 / *Published:* 10 August 2020

To enhance the photocatalytic performance of zinc oxide materials, nitrogen doped zinc oxide (ZnO:N) nanosheets with mesoporous structure, are prepared by a facile homogeneous precipitation technique. The nanosheets are micron-sized and have a thickness of about 15 nm, and they exhibit a two-dimensional mesoporous network structure that is constructed by interconnected strip-like nanoparticles of about 20 nm in width. As a photocatalyst, the nitrogen doping can reduce the optical band gap of zinc oxide, and the mesoporous network structure can increase the absorption and photochemical reaction interfaces. Consequently, mesoporous ZnO:N nanosheets exhibit significantly improved photocatalytic activity for the photodegradation of rhodamine B (RhB) as well as enhanced photoelectrochemical performance than those of commercial ZnO particles, confirming that the design of material structure and composition is quite effective.

Keywords: Zinc oxide; Nitrogen doping; Mesoporous; Nanosheet; Photocatalytic activity

1. INTRODUCTION

To reduce the environmental pollution caused by organic contaminants, photocatalytic degradation using semiconductor photocatalysts is an effective method [1−3]. As one of the most important semiconductor photocatalysts, ZnO has attracted much attention due to its excellent properties, such as high electron mobility, good stability, nontoxicity, and low cost [4−6]. However, its practical application is severely limited due to the wide theoretical band gap of 3.37 eV and the fast recombination of photogenerated carriers. To enhance the photocatalytic performance, various approaches have been developed. For example, doping with metallic/nonmetallic elements [7−10], forming heterojunctions [11,12], incorporating with noble metal nanoparticles [13−15] and introducing oxygen vacancies [16] have been used to reduce the optical band gap and/or suppress the recombination of carries, and in addition, preparing nanostructures [17,18] has been adopted to enlarge the adsorption and reaction

interfaces for enhancing the kinetics. Therefore, in the past decades, a lot of ZnO-based photocatalysts with different nanostructures, such as porous structure [19,20], micro/nanorods [21−23], nanosheets [24,25], nanoflowers [26,27], micro/nanospheres [28,29], and so on, have been designed and applied. Among these nanostructured materials, mesoporous materials are crucial and they show advantages of ultra-high specific surface area, large pore volume, narrow pore size distribution, regular channel structure, as well as significant nano-size effect in the pore structure [30], so they are often well-designed to maximize the photocatalytic activity. However, the preparation of mesoporous materials is usually quite complicated and often needs the assistance of surfactants and/or templates, which are sometimes difficult to remove completely.

Therefore, in the present work, a facile homogeneous precipitation method is developed to fabricate mesoporous nitrogen doped zinc oxide (ZnO:N) nanosheets, and the photocatalytic activity of the product is investigated in detail.

2. EXPERIMENTAL

2.1. Sample preparation

Mesoporous ZnO:N nanosheets were prepared by a homogeneous precipitation technique. Deionized water (pH = 7.50) was used as the solvent. In a 200 mL beaker, 7.5 mmol zinc nitrate hexahydrate and 150 mmol urea were dissolved in 150 mL water to obtain a solution with the pH value of about 6.00. The beaker was sealed with several layers of filter paper and placed in a water bath of 80 °C for 4 h under mildly stirring. A homogeneous precipitation reaction occurred in the solution, and the resultant white precipitate was collected by centrifugation at 2000 rpm for 3 min. The precipitate was centrifugally washed with just 25 mL water for only twice, and the pH of the final clear solution rose to 6.85. Afterwards, the precipitate was dried at 80 °C, calcined in a tube furnace at 350 °C in air for 45 min, and a fine light-yellow powder was produced.

2.2. Materials characterizations

The microstructure and morphology of the materials were characterized by means of X-ray diffraction (XRD, Bruker D8 advance; Cu Kα radiation), scanning electron microscopy (SEM, Hitachi S–4800, equipped with energy dispersive spectrometer (EDS)) and transmission electron microscopy (TEM, FEI Tecnai G2 F20). The optical properties were determined by ultraviolet-visible diffuse reflectance spectroscopy (UV-vis DRS) on a spectrophotometer (Hitachi U−4100) in the wavelength range between 200 and 800 nm.

2.3. Photocatalytic activity tests

The photocatalytic activity of mesoporous ZnO:N nanosheets was evaluated by the photodegradation of RhB aqueous solution. In a quartz-glass test tube, 20 mg ZnO:N was dispersed uniformly into 40 mL RhB solution with the concentration of 10 mg L^{-1}. The suspension was stirred in

the dark for 30 min before illumination to ensure that the catalyst fully absorbed the dye. Under continuously stirring, the mixture was irradiated by UV light (300 W mercury lamp) at a constant temperature of 25 °C maintained by a cooling-water circulation machine. At an interval of five minutes, 4 mL suspension was sampled and centrifuged to remove the catalyst. The clear solution was transferred into a quartz-glass cuvette and analyzed by UV-vis absorption spectroscopy on a spectrophotometer (Shimadzu UV–2700) to determine the residual RhB concentration. At the same time, commercial ZnO, TiO_2 (P25) and a blank experiment without adding catalyst were tested for comparative evaluation.

2.4. Photoelectrochemical measurements

Photoelectrochemical tests were performed on an electrochemical workstation (CHI660E) using a three-electrode cell with a quartz-glass window. The catalyst ink was prepared by dispersing 4 mg photocatalyst homogeneously into a solution mixed by 1 mL 5 wt% Nafion solution, 7 mL ethanol and 2.5 mL water. 150 μL ink was dropped onto an indium tin oxide (ITO) glass with an exposed area of 0.5 cm^2, and then dried in air and further heated at 200 °C to fabricate the working electrode. To assemble the cell, the working electrode was placed in front of the quartz-glass window, a Pt foil was used as the counter electrode, a Hg/Hg_2SO_4 electrode was used as the reference electrode and a solution of 0.5 M Na_2SO_4 was used as the electrolyte. Photocurrent responses were tested by irradiating the working electrode periodically by switching on/off the 300 W Xenon lamp at an interval of 30 s. Electrochemical impedance spectroscopy (EIS) was investigated on the same system under the light irradiation over a frequency range of 0.01 to 100 kHz using a voltage signal of 5 mV in amplitude.

3. RESULTS AND DISCUSSION

The XRD pattern of the ZnO:N sample is presented in Figure 1. All diffraction peaks can be perfectly indexed to the atomic planes of wurtzite-type hexagonal ZnO, according to JCPDS no. 36–1451, suggesting that the doping of nitrogen into ZnO does not produce new phases. The relatively broad diffraction peaks indicate that the sample has fine grains.

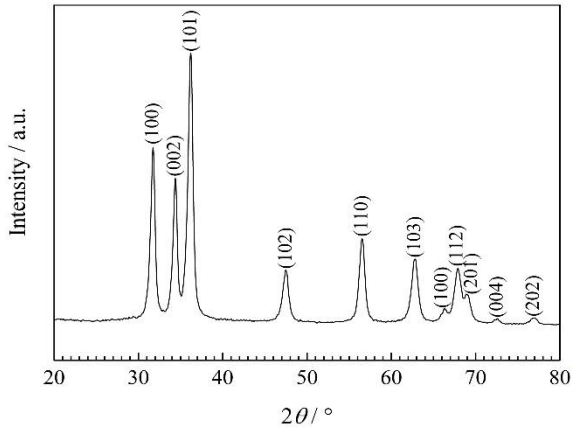

Figure 1. The XRD pattern of the mesoporous ZnO:N nanosheets.

The SEM results of the ZnO:N sample are shown in Figure 2. The sample exhibits a nanosheet structure (Figure 2a). These nanosheets are micron-sized in length/width and show a good dispersion without stacking. According to the high-magnification image (Figure 2b), the nanosheets are assembled by interconnected strip-like nanoparticles, and most of the pores among them are less than 50 nm, forming a two-dimensional mesoporous network structure. It can be measured from an upright nanosheet that the thickness is only about 15 nm. To study the elemental composition of the material, the powder was compressed into a tablet under a pressure of 20 MPa and then qualitatively analyzed by means of EDS. The resultant pattern (Figure 2c) shows that apart from the peaks of Zn and O, the peak of N located at about 0.39 keV can also been distinguished, with the weak intensity due to the low content.

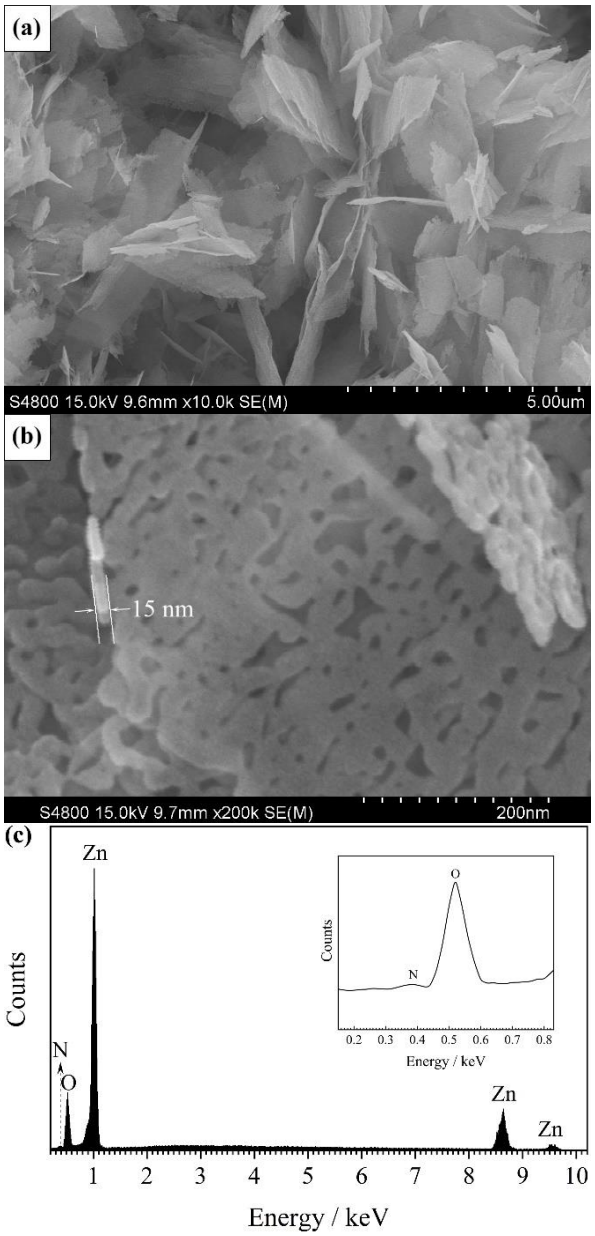

Figure 2. The SEM results of the mesoporous ZnO:N nanosheets: (a) the image at low magnification, (b) the image at high magnification and (c) the EDS pattern.

The nanostructure of the mesoporous nanosheet was further characterized by TEM, as shown in Figure 3. The TEM image of a portion of a nanosheet (Figure 3a) confirms its two-dimensional mesoporous network structure. The constituent strip-like nanoparticles are interconnected with each other, having an average width of about 20 nm, and most of the pores among the nanoparticles range between 10 and 50 nm in size. Figure 3b presents the corresponding selected area electron diffraction (SAED) pattern. It exhibits only one group of diffraction rings that can be well indexed to the atomic planes of wurtzite structured ZnO, indicative of the single phase and its polycrystalline nature. Figure 3c gives the high-resolution TEM image of a constituent nanoparticle, which reveals a clear lattice spacing of 0.248 nm, consistent with the spacing value of (101) atomic planes of ZnO. All these characterization results confirm that the mesoporous nitrogen doped zinc oxide has been prepared successfully.

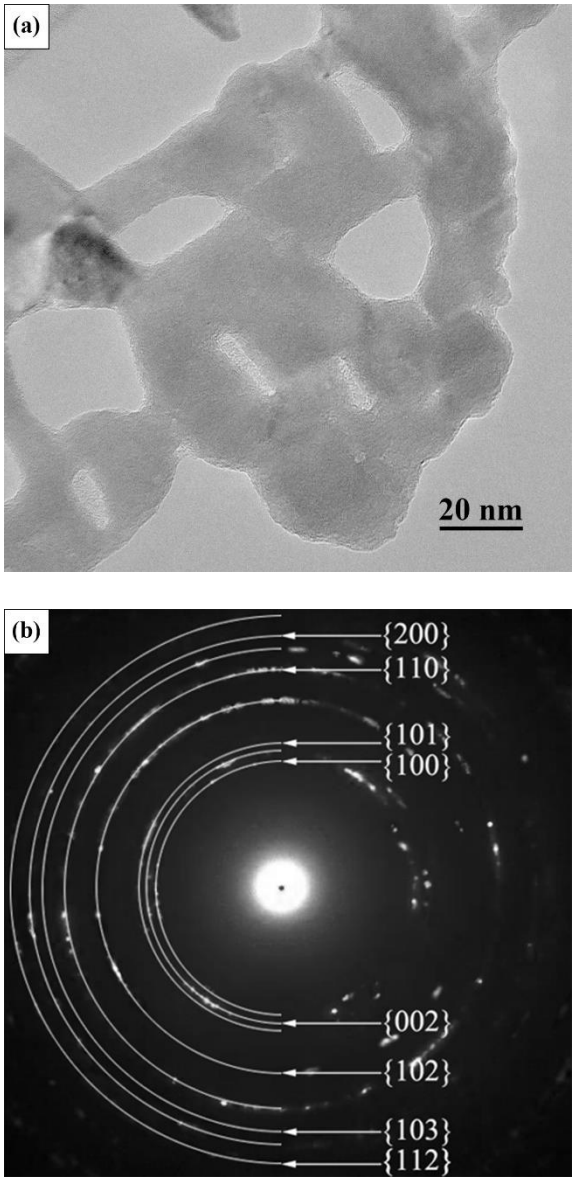

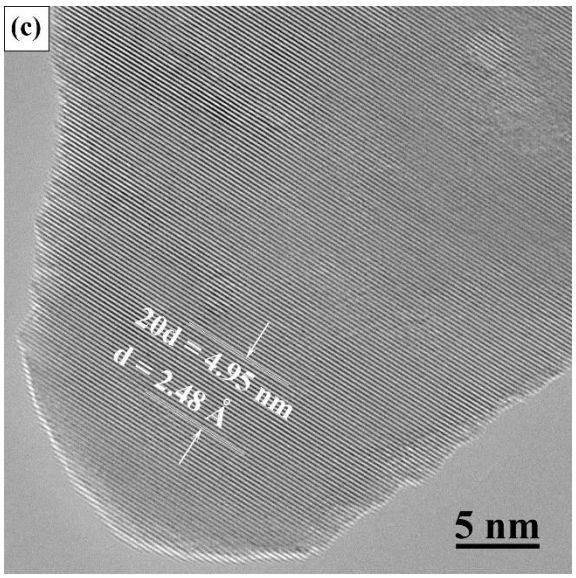

Figure 3. The TEM results of the mesoporous ZnO:N nanosheets: (a) the TEM image of the nanosheet, (b) the corresponding SAED pattern and (c) the HRTEM image of a constituent nanoparticle.

The characterization results of the commercial ZnO sample are presented in Figure 4. The XRD pattern (Figure 4a) shows only one set of sharp diffraction peaks of ZnO, indicative of high purity and good crystallinity. The SEM image (Figure 4b) shows that the powder consists of irregular solid particles with submicron sizes.

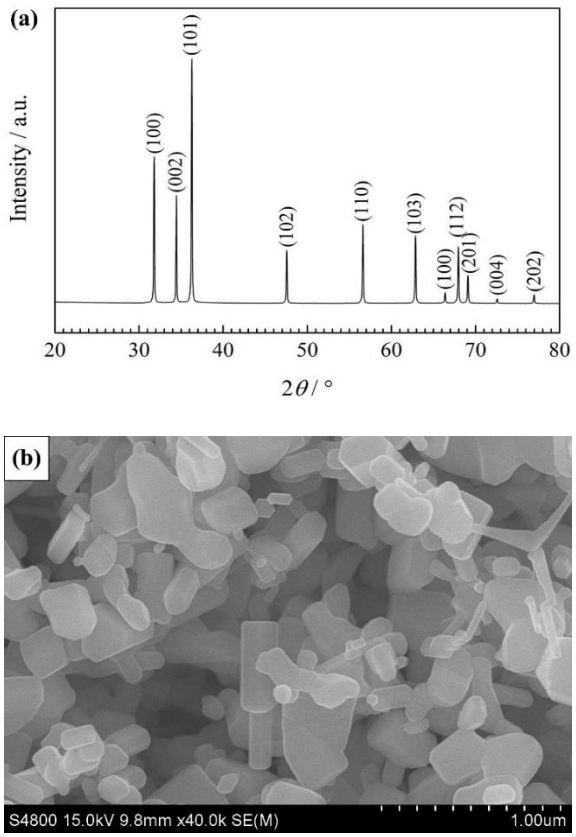

Figure 4. (a) The XRD pattern and (b) SEM image of the commercial ZnO powder.

Figure 5 compares the UV-vis DRS results of the mesoporous ZnO:N nanosheets and the commercial ZnO particles. In their spectra (Figure 5a), both samples show strong absorptions in the ultraviolet region. However, the mesoporous nanosheets exhibit an enhanced optical absorbance in the visible light region and show a slight red shift of the absorption edge. The inserted photos compare the actual colors of two samples, showing that the commercial ZnO sample is white, whereas the ZnO:N sample is light yellow, and the color change of the ZnO:N sample is originated from the nitrogen doping [31]. Their color differences can be reflected in their spectra, as the ZnO:N sample have stronger absorption in the blue light range. A plot of $(\alpha h\nu)^2$ versus $h\nu$ can be established for the calculation of optical band gap, and the resulting curves of the two samples are shown in Figure 5b. The intercept of the extension line of the linear part of the curve on the horizontal axis can be determined as the optical band gap [3,10]. The value obtained by this method for the ZnO:N sample is 3.08 eV, lower than that of the commercial ZnO particles (3.20 eV). This indicates that the nitrogen doping reduces the optical band gap of the zinc oxide material, because it introduces defect energy levels in the forbidden band.

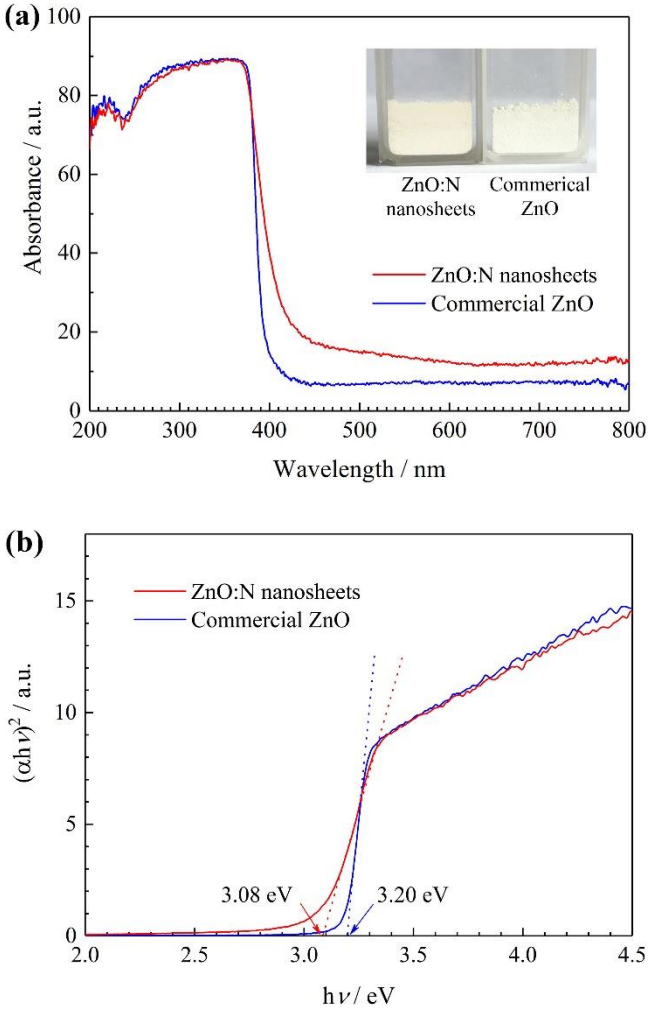

Figure 5. (a) UV–vis diffuse reflectance spectra of the mesoporous ZnO:N nanosheets and the commercial ZnO particles and (b) the corresponding plots of $(\alpha h\nu)^2$ versus $h\nu$ of the two samples.

The photocatalytic activities of the samples are investigated by the degradation of RhB solution under the irradiation of UV light. Figure 6 compares the UV-vis absorption spectra of the RhB solution photodegraded by the ZnO:N and ZnO catalysts after different irradiation time. The maximum absorption peaks in the spectra at 553 nm decrease gradually with the illumination time, and accordingly, the color of the solution gradually becomes lighter. For the solution containing ZnO:N catalyst (Figure 6a), the peak almost disappears and the solution becomes colorless after 25 min, suggesting that the RhB has been almost completely degraded. However, for the solution containing commercial ZnO catalyst (Figure 6b), this process takes as long as 60 min.

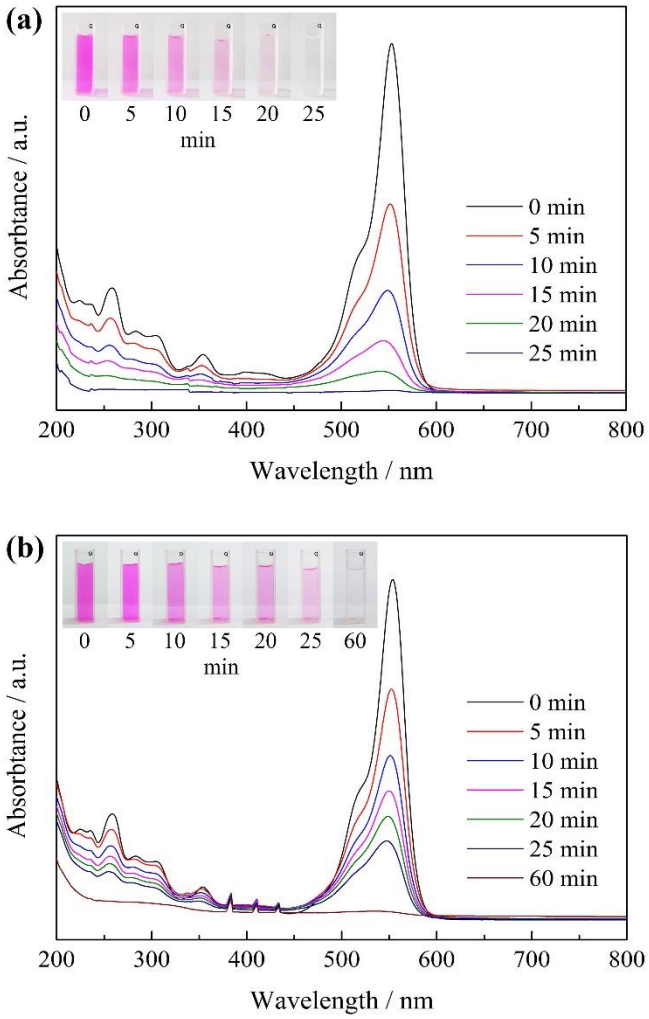

Figure 6. The UV–vis absorption spectra of the RhB solutions after different UV-light irradiation time in the presence of (a) the mesoporous ZnO:N nanosheets and (b) the commercial ZnO particles. The inserted photos show their color changes with the irradiation time.

The photodegradation curve of RhB solution in the presence of the mesoporous ZnO:N nanosheets is displayed in Figure 7. For comparison, the curves showing the degradation of RhB by commercial ZnO powder, commercial TiO_2 powder (P25) and a blank experiment (no catalyst) are also presented together. The residual concentration of RhB (C_i) is determined by the main absorbance centered at 553 nm. In the absence of catalyst, the decrease in the RhB concentration is extremely low,

indicating that the photoinduced self-degradation can be neglected. The use of catalysts can significantly accelerate the degradation rate. After the illumination for 25 min, the degradation efficiency of RhB by the ZnO:N catalyst is 99.6%, which is slightly higher than that of the TiO_2 (P25) powder (96.4%), but much higher than that of the pure ZnO powder (only 76.9%), indicative of significantly enhanced photocatalytic activity.

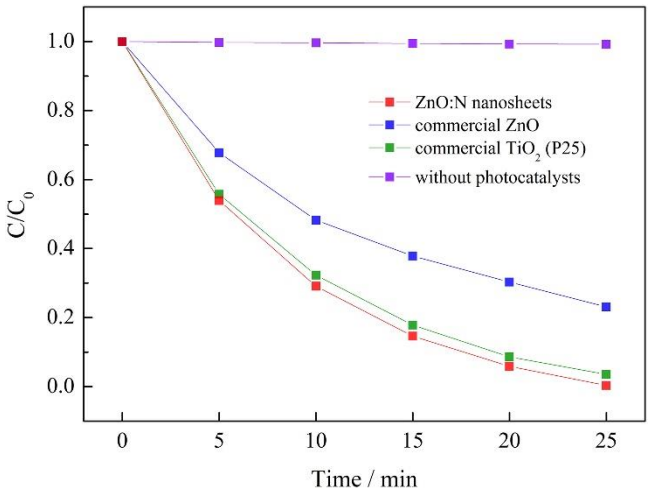

Figure 7. Photodegradation curves of RhB by different catalysts under UV-light irradiation. (0.5 g L^{-1} photocatalyst, 10 mg L^{-1} RhB and 300 W Hg lamp).

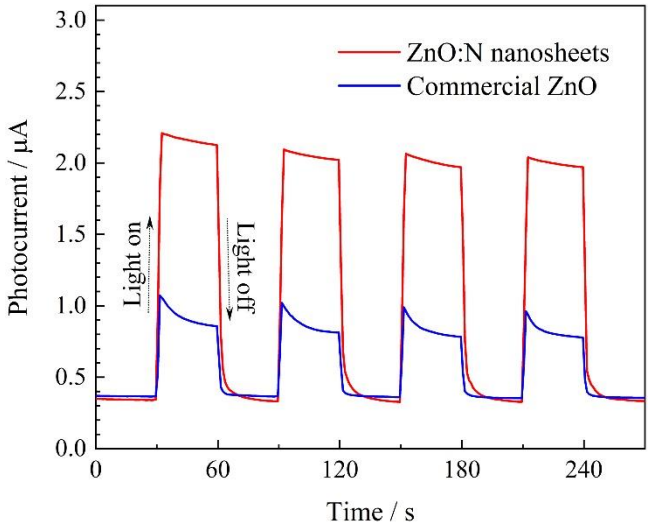

Figure 8. Photocurrent responses of the ZnO:N and ZnO electrodes.

The photocurrent responses of the ZnO:N and ZnO electrodes under intermittent illumination are compared in Figure 8. When the light is switched on, the photocurrents rise immediately. It is well known that photocurrent is generated by the migration of photo-generated electrons and holes. Higher photocurrent corresponds to more efficient carrier separation and migration, which leads to higher photocatalytic activity [32]. At each stage of light radiation, the ZnO:N electrode shows a photocurrent

about three times as high as that of the ZnO electrode, indicative of an enhanced electron-hole separation and migration.

Figure 9 shows the comparison of EIS Nyquist plots of two electrodes. Both samples show a semicircle in the medium-frequency region, which is related to the charge transfer impedance on the electrode/electrolyte interface. The smaller diameter of the semicircle for the ZnO:N electrode relative to the ZnO electrode indicates a lower charge-transfer impedance [32, 33]. This result also confirms that the separation and migration of carriers in the ZnO:N sample are more effective.

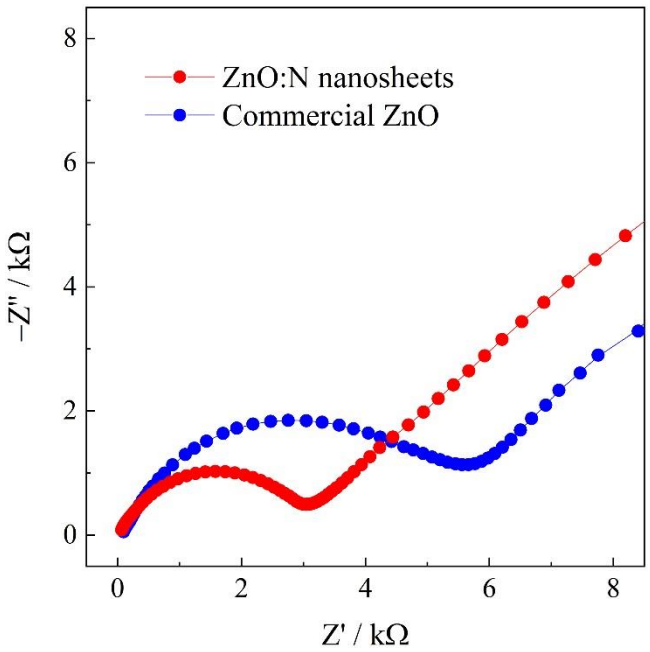

Figure 9. Nyquist plots of the ZnO:N and ZnO electrodes (frequency range: 0.01–100 kHz).

The enhanced photocatalytic performance is ascribed to the nitrogen doping and the mesoporous nanosheet structure. First, the doping of nitrogen reduces the optical band gap of ZnO, allowing it to absorb a larger proportion of light and generate more photo-generated electron-hole pairs during the light exposure, and thereby generating more hydroxyl radicals and improving the ability of oxidative degradation of pollutants. Second, the mesoporous nanosheet structure can shorten the migration distance of the photon-generated carriers to the particle surface, so it can effectively increase the separation efficiency, reduce their recombination, and allow more carriers to participate in the photochemical reaction. Third, the mesoporous nanosheet structure has advantages of larger pore volume and higher specific surface area, so it can increase the dye absorption and enlarge the photochemical reaction interfaces to accelerate the reaction rate. Fourth, the good dispersion of the nanosheets and their mesoporous network structure prevent the constituent nanoparticles from agglomerating, so each nanoparticle can participate more fully in the photochemical reaction. All these factors are advantageous to the photochemical reaction kinetics, and as a result, the photocatalytic performance of mesoporous ZnO:N nanosheets is enhanced.

Because of the above-mentioned structure and component advantages, compared with many previously reported ZnO-based photocatalysts, this mesoporous ZnO:N nanosheets exhibits competitive

photocatalytic performance, as shown in Table 1. The enhancement in photocatalytic performance confirms the effectiveness of the material design, which can also be applied to other photocatalytic materials.

Table 1. Comparison of photocatalytic activities between some previously reported ZnO-based samples and the mesoporous ZnO:N nanosheets in the present work.

Photocatalyst	Loading	RhB concentration	Irradiation condition	Degradation	Reference
ZnO microcubes	0.36 g L^{-1}	10 mg L^{-1}	UV, 300 W, 120 min	98.1%	[34]
ZnO microspheres	1 g L^{-1}	10 mg L^{-1}	UV, 500 W, 70 min	≈ 99.6%	[35]
ZnO nanocrystals	0.8 g L^{-1}	6 mg L^{-1}	UV, 125 W, 100 min	≈ 84.0%	[36]
Rose-like ZnO	0.4 g L^{-1}	10 mg L^{-1}	UV, 300 W, 25 min	99.84%	[37]
Flower-like ZnO	0.3 g L^{-1}	4.79 mg L^{-1}	UV, 200 W, 100 min	≈ 98.5%	[38]
ZnO/TiO_2 nanofibers	0.2 g L^{-1}	10 mg L^{-1}	UV, 250 W, 50 min	≈ 99.1%	[39]
ZnO:Ce microflowers	2 g L^{-1}	8 mg L^{-1}	UV, 175 W, 120 min	≈ 69.5%	[40]
ZnO:N nanosheets	0.5 g L^{-1}	10 mg L^{-1}	UV, 300 W, 25 min	99.6%	This work

4. CONCLUSIONS

In summary, mesoporous ZnO:N nanosheets have been successfully prepared by homogenous precipitation technique. The nanosheets exhibit a two-dimensional mesoporous network structure that is constructed by interconnected strip-like nanoparticles. As a photocatalyst, mesoporous ZnO:N nanosheets exhibit enhanced photocatalytic performance for the degradation of rhodamine B (RhB) compared with that of commercial ZnO particles. The enhancement is attributed to the nitrogen doping and the mesoporous nanosheet structure, as they can reduce the optical band gap of zinc oxide, reduce the recombination of carriers, and enhance the photochemical reaction kinetics.

ACKNOWLEDGMENTS
This work is supported by Zhejiang Provincial Natural Science Foundation of China (Grant No. LTY20E010001). We would like to acknowledge it for financial support.

References

1. S.W. Cao, J.X. Low, J.G. Yu and M. Jaroniec, *Adv. Mater*., 27 **(**2015) 2150.
2. H.L. Tan, R. Amal and Y.H. Ng, *J. Mater. Chem. A*, 5 (2017) 16498.
3. V. Kurnaravel, S. Mathew, J. Bartlett and S.C. Pillai, *Appl. Catal. B-Environ.*, 244 (2019) 1021.
4. K.Z. Qi, B. Cheng, J.G. Yu and W.K. Ho, *J. Alloy. Compd.*, 727 (2017) 792.
5. L.Q. Fan, J.H. Wang, N. Qiu, Y. Liu and X.M. Zhang, *Int. J. Electrochem. Sci.*, 14 (2019) 10862.
6. L.L. Wang, W. Ma, J.L. Ma and G.Q. Shao, *Int. J. Electrochem. Sci.*, 14 (2019) 9150.
7. B.M. Rajbongshi, A. Ramchiary and S.K. Samdarshi, *Mater. Lett.*, 134 (2014) 111.
8. W.L. Yu, J.F. Zhang and T.Y. Peng, *Appl. Catal. B-Environ*., 181 (2015) 220.

9. A.N. Kadam, T.G. Kim, D.S. Shin, K.M. Garadkar and J. Park, *J. Alloy. Compd.*, 710 (2017) 102.
10. Y. Zhang, J.B. Zhou, X. Chen, Q.Q. Feng and W.Q. Cai, *J. Alloy. Compd*., 777 (2019) 109.
11. K. Ravichandran, K. Kalpana, R. Uma, E. Sindhuja and K. Shantha seelan, *Mater. Res. Bull.*, 99 (2018) 268.
12. Y.J. Liu, H.X. Liu, H.M. Zhou, T.D. Li and L.N. Zhang, *Appl. Surf. Sci*., 466 (2019) 133.
13. Y.Q. Yang, H.X. Li, F.L. Hou, J.Y. Hu, X.D. Zhang and Y.X. Wang, *Mater. Lett.*, 180 (2016) 97.
14. S. Koppala, Y. Xia, L.B. Zhang, J.H. Peng, Z. Chen and L. Xu, *Ceram. Int*., 45 (2019) 15116.
15. H.F. Liu, L.L. Zhong, S. Govindaraju and K. Yun, *J. Phys. Chem. Solids*, 129 (2019) 46.
16. H.L. Guo, Q. Zhu, X.L. Wu, Y.F. Jiang, X. Xie and A.W. Xu, *Nanoscale*, 7 (2015) 7216.
17. H. Tong, S.X. Ouyang, Y.P. Bi, N. Umezawa, M. Oshikiri and J.H. Ye, *Adv. Mater.*, 24 (2012) 229.
18. A. Kubacka, M. Fernandez-Garcia and G. Colon, *Chem. Rev.*, 112 (2012) 1555.
19. X.L. Ren, H.L. Hou, Z.X. Liu, F.M. Gao, J.J. Zheng, L. Wang, W.G. Li, P.Z. Ying, W.Y. Yang and T. Wu, *Small*, 12 (2016) 4007.
20. K. Vignesh, S. Kang, B.S. Kwak and M. Kang, *Sep. Purif. Technol.*, 147 (2015) 257.
21. H.L. Lv, G.B. Ji, Z.H. Yang, Y.S. Liu, X.M. Zhang, W. Liu and H.Q. Zhang, *J. Colloid Interface Sci*., 450 (2015) 381.
22. R. Raji, K.S. Sibi and K.G. Gopchandran, *Appl. Surf. Sci.*, 427 (2018) 863.
23. J. Al-Sabahi, T. Bora, M. Al-Abri and J. Dutta, *Materials*, 9 (2016) 238.
24. S. Kumar, N.L. Reddy, A. Kumar, M.V. Shankar and V. Krishnan, *Int. J. Hydrogen Energy*, 43 **(**2018) 3988.
25. Y. Chen, J. Li, B.Y. Zhai and Y.N. Liang, *Colloids Surf. A Physicochem. Eng. Asp.*, 568 (2019) 429.
26. Y. Xu, J.J. Jin, X.L. Li, Y.D. Han, H. Meng, T.Y. Wang and X. Zhang, *Mater. Res. Bull.*, 76 (2016) 235.
27. S.M. Lam, J.A. Quek and J.C. Sin, *Mater. Lett.* 195 (2017) 34.
28. J.Q. Qin, X.Y. Zhang, C.W. Yang, M. Cao, M.Z. Ma and R.P. Liu, *Appl. Surf. Sci.*, 392 (2017) 196.
29. N. Nie, L.Y. Zhang, J.W. Fu, B. Cheng and J.G. Yu, *Appl. Surf. Sci.*, 441 (2018) 12.
30. Q. Han, B. Wang, J. Gao, Z.H. Cheng, Y. Zhao, Z.P. Zhang and L.T. Qu, *ACS Nano*, 10 (2016) 2745.
31. M. Zheng and J.Q. Wu, *Appl. Surf. Sci.*, 255 (2009) 5656.
32. S. Wang, B.C. Zhu, M.J. Liu, L.Y. Zhang, J.G. Yu and M.H. Zhou, *Appl. Catal. B-Environ.*, 243 (2019) 19.
33. I. Ahmad, M.S. Akhtar, E. Ahmed, M. Ahmad, V. Keller, W.Q. Khan and N.R. Khalid, *Sep. Purif. Technol.*, 237 (2020) 116328.
34. J.J. Ban, G.C. Xu, L. Zhang, H. Lin, Z.P. Sun, Y. Lv and D.Z. Jia, *J. Solid State Chem.*, 256 (2017) 151.
35. Y.X. Guo, S.W. Lin, X. Li and Y.P. Liu, *Appl. Surf. Sci.*, 384 (2016) 83.
36. Y. Zhou, LH. Xu, Z.J. Wu, P. Li and J.J. He, *Optik*, 310 (2017) 673.
37. Y. Miao, H.J. Zhang, S. Yuan, Z. Jiao and X.D. Zhu, *J. Colloid Interface Sci.*, 462 (2016) 9.
38. B.X. Li and Y.F. Wang, *J. Phys. Chem. C*, 114 (2010) 890.
39. J. Li, L. Yan, Y.F. Wang, Y.H. Kang, C. Wang and S.B. Yang, *J. Mater. Sci: Mater. Electron.*, 27 (2016) 7834.
40. Y.M. Liang, N. Guo, L.L. Li, R.Q. Li, G.J. Ji and S.C. Gan, *RSC Adv.*, 5 (2015) 59887.